Accepted Manuscript

One step synthesis of high efficiency nickel/mesoporous TiO$_2$ hybrid catalyst for hydrogen evolution reaction

Esteban A. Franceschini , Melisa J. Gomez , Gabriela I. Lacconi

Please cite this article as: Esteban A. Franceschini , Melisa J. Gomez , Gabriela I. Lacconi , One step synthesis of high efficiency nickel/mesoporous TiO$_2$ hybrid catalyst for hydrogen evolution reaction, *Journal of Energy Chemistry* (2018), doi: 10.1016/j.jechem.2018.02.005

One step synthesis of high efficiency nickel/mesoporous TiO$_2$ hybrid catalyst for hydrogen evolution reaction

Esteban A. Franceschini[a,b,*], Melisa J. Gomez[a], Gabriela I. Lacconi[a]

[a] *INFIQC-CONICET, Dto. de Fisicoquímica – Facultad de Ciencias Químicas, Universidad Nacional de Córdoba, Ciudad Universitaria, 5000, Córdoba, Córdoba, Argentina*

[b] *Departamento de Física de la Materia Condensada, Centro Atómico Constituyentes, Comisión Nacional de Energía Atómica, B1650KNA San Martín, Buenos Aires, Argentina*

[*] Corresponding author. Fax: 54 0351 433 4188

   E-mail address: estebanfranceschini@yahoo.com.ar (E. Franceschini).

ABSTRACT

Nickel-TiO$_2$ hybrid catalysts are synthesized by electrodeposition and their catalytic activity with respect to the hydrogen evolution reaction is analyzed. Two types of titanium oxide particles, which are commercial particles of dense TiO$_2$ and mesoporous TiO$_2$ particles synthesized by an aerosol method, are incorporated into the matrix of the nickel catalyst,. Both nickel catalysts containing TiO$_2$ particles presented higher catalytic activity than the conventional nickel Watts catalyst. Mesoporous TiO$_2$-modified nickel catalyst showed the highest catalytic activity towards HER in alkaline medium. In addition, this type of nickel catalyst increases its catalytic activity after ageing treatment, which is an indication of an increase in the electro-active area of the electrode.

Keywords: Co-deposition; Impedance spectroscopy; Titanium oxide; Ageing process; Raman spectroscopy

1. Introduction

In the last decades hydrogen has attracted much attention from the scientific community as a vector of clean energy that can be easily obtained using alternative energy sources [1–4]. It is of particular interest the preparation by means of water electrolysis in alkaline medium as it allows the production of high purity hydrogen using non-noble metal catalysts, markedly reducing the cost of the hydrogen produced [5,6]. In this sense, nickel or modified nickel electrodes have been presented numerous times as viable alternatives [7–10].
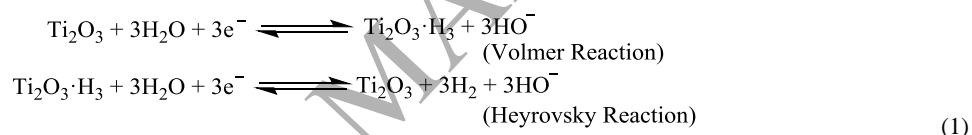
In recent years, nickel-based hybrid electrodes have attracted attention since they have particular properties, possibly due to a synergistic effect between the materials used [11–13]. It has been reported in literature that the use of TiO$_2$ as a modifying agent of the nickel matrix substantially improves the catalytic activity of the electrode towards the hydrogen evolution reaction (HER) [14,15].

Typically, nickel/TiO$_2$ composites are used in the generation of photocatalyzed hydrogen [16,17], although in recent years some work has been presented on the generation of conventional electrochemical hydrogen using this
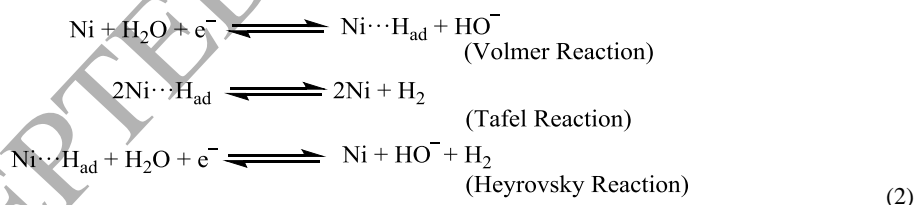
1

type of catalysts. Lasia and coworkers [14] synthesized Ni-P-TiO$_2$ catalysts on copper supports by a method of codeposition and found that the presence of TiO$_2$, and possibly accompanied by the non-stoichiometric oxide of Ti$_2$O$_3$, increased the catalytic activity of the electrode with respect to HER. Elias and Hegde [18] reported the modification of nickel catalysts with TiO$_2$ particles by modifying a citrate nickel bath using glycerol as additive, by anodic dissolution and TiO$_2$ nanoparticles incorporation. The highest electrocatalytic character of Ni-TiO$_2$ composite coating was attributed to a synergistic effect related to the high number of electroactive centers affected by TiO$_2$ nanoparticles incorporation.

The implementation of mesoporous materials in electrocatalysis has allowed in recent years to considerably increase the real electrochemical area of the catalysts used and, therefore, their effective catalytic activity [19,20]. Particularly, the mesoporous materials of TiO$_2$ are of great interest since these materials can be obtained in the form of mesoporous particles by methods that allow the continuous synthesis of particles [21].

The synergetic effect above-mentioned on the HER kinetics on the Ni + TiO$_2$ electrodes, responsible for the higher electrode activity, arises not only from the presence of TiO$_2$, but from the existence of a layer of non-stoichiometric titanium oxide, Ti$_2$O$_3$, formed on the boundary of the TiO$_2$ grains that present an electrocatalytic effect on the HER according to equations (1) [14]:

$$Ti_2O_3 + 3H_2O + 3e^- \rightleftharpoons Ti_2O_3 \cdot H_3 + 3HO^- \quad \text{(Volmer Reaction)}$$
$$Ti_2O_3 \cdot H_3 + 3H_2O + 3e^- \rightleftharpoons Ti_2O_3 + 3H_2 + 3HO^- \quad \text{(Heyrovsky Reaction)} \tag{1}$$

coupled to the Volmer, Heyrovsky and Tafel steps occurring on nickel:

$$Ni + H_2O + e^- \rightleftharpoons Ni\cdots H_{ad} + HO^- \quad \text{(Volmer Reaction)}$$
$$2Ni\cdots H_{ad} \rightleftharpoons 2Ni + H_2 \quad \text{(Tafel Reaction)}$$
$$Ni\cdots H_{ad} + H_2O + e^- \rightleftharpoons Ni + HO^- + H_2 \quad \text{(Heyrovsky Reaction)} \tag{2}$$

In this work we present nickel/TiO$_2$ hybrid catalysts synthesized by a simple and reproducible method using different types of TiO$_2$ particles with different morphologies. Of particular interest is the development of advanced materials that can be synthesized simply and without major modifications of the industrial processes currently used for the synthesis of electrodes. Particularly the method used in this work consists in the direct modification of a conventional bath of Watts for the obtaining of nanostructured catalysts of great efficiency. The nickel Watts catalyst is the material obtained conventionally by means of an electrodeposition bath containing NiSO$_4$, NiCl$_2$ and boric acid to maintain the pH in 3.5 (denoted as "nickel Watts bath"). This bath allows to obtain electrodeposits of rough nickel which is normally used as catalyst in conventional alkaline electrolyzers. Two types of TiO$_2$ particles, commercial TiO$_2$ particles with an anatase-like structure and mesoporous TiO$_2$ aerosols with an amorphous structure were used

2

for the modification of the nickel Watts bath. The synthesized materials were tested for the hydrogen generation in alkaline medium, studying also the decay in the catalytic activity due to the ageing process by formation of surface nickel hydrides.

2. Experimental

2.1. Materials

Nickel chloride hexahydrate (Merck, PA grade), nickel sulfate hexahydrate (Anedra, PA grade), boric acid (Merck, PA grade), hydrochloric acid (36.5%−37%, Cicarelli, PA grade), ethanol (96%, Cicarelli, PA grade), potassium hydroxide (Anedra RA reagent), titanium dioxide (ReagentPlus®, ≥99%, Sigma-Aldrich), triblock poly(ethylene oxide)–b–poly(propylene oxide)–b–poly(ethylene oxide) copolymer $EO_{106}PO_{70}EO_{106}$, denoted Pluronic F127® (M_w = 12,600 Da, Aldrich), Titanium(IV) isopropoxide (Aldrich, 97%), glacial acetic acid (Merk), acetylacetonate (denoted as ACAC, Merk), were used as received. All solutions were prepared with Milli-Q water, and degassed employing high purity N_2 (Indura S.A.).

2.2. Electrodeposition baths preparation

The catalysts were synthesized using a conventional nickel Watts bath which was modified by the addition of two types of TiO_2 particles, to analyze the differences generated in the hybrid catalyst by the presence of mesopores in the TiO_2 matrix. For that, 25 g of boric acid were dissolved in water at 323 K, 240 g of nickel sulfate hexahydrate and then 25 g of nickel chloride hexahydrate were added to the boric acid solution under constant stirring to obtain 1 L of solution. Finally, 65 mL of Watts solution was taken and 0.2 g of the TiO_2 powder was added to obtain electrodeposition baths for nickel/dense TiO_2 ($NiTiO_{2dense}$) and nickel/ mesoporous TiO_2 ($NiTiO_{2mesop}$) electrodes.

2.3. Characterization

2.3.1. Chemical and structural characterization

SEM micrographs were obtained using a Supra 40 FESEM (Zeiss Company) operating at 8 kV equipped with EDX (Oxford). The X-ray diffractograms were obtained using the λ = 1.5406 Å Cu $K\alpha$ radiation, with a PANalytical X'Pert PRO diffractometer operating at 40 kV and 40 mA, in the $\theta - 2\theta$ Bragg–Brentano geometry. The 2θ range used was between 10° and 70°, with 0.02° steps and counting time of 2 s per step at room temperature. The crystal structure was refined using the Rietveld method employing the FULLPROF program [22] and a pseudo-Voigt shape function was used to fit the experimental data. The data refined were atomic positions, isotropic thermal parameters, lattice parameters, peak shape, and occupation factors.

Raman spectra were acquired with a LABRAM-HR, Horiba Jobin-Yvon Raman microscope with a 100 x objective lens (NA = 0.9). The Ar laser excitation was 488.0 nm with 3.5 mW power in order to avoid laser induced heating. The illuminated area in all Raman experiments was 1.0 μm^2 with a spectral resolution of 1.5 cm^{-1} and at least five different zones on each sample were analyzed.

2.3.2. Electrochemical characterization

All the electrochemical characterizations were made in a three-electrode electrochemical cell equipped with a thermostatic jacket using a 1 M KOH aqueous solution as electrolyte. During the entire electrochemical measurements a high purity N_2 flux was maintained over the electrolyte surface to deaerate the solution. A large area platinum foil was used as counter electrode and a saturated calomel electrode (SCE) as reference electrode (0.243 V vs. RHE). The temperature of the electrochemical cell was varied between 298 K and 323 K using a Lauda Alpha RA 8 controller. On the other hand, the reference electrode was kept at room temperature by maintaining it out the electrochemical cell and the circuit was closed using a capillary luggin.

The electrochemical experiments were carried out employing an Autolab PGStat30 potentiostat/galvanostat coupled to a FRA2 module. The uncompensated ohmic drop correction was conducted as presented elsewhere [23]. The area used for all current densities calculation was 0.196 cm^2 (the geometric area of the disk electrode). Cyclic voltammetry (CV) experiments were carried out between 0.1 and −1.5 V (vs. SCE) at a scan rate of 10 mV s^{-1} for all electrodes.

Electrochemical impedance spectroscopy (EIS) experiments were made at frequencies between 10 mHz and 100 kHz using a 10 mV bias potential at different electrode potentials (open circuit potential (OCP), HER onset potential (OP), 0.1 V and 0.3 V more cathodic than the corresponding OP of each catalyst) in order to cover the potential range where the HER occurs [22]. The ZView 3.3 software (Scribner Associates, Inc.) was used to fit the measured data with different equivalent circuit models.

Chronoamperometric profiles were measured by applying a potential pulse of −1.5 V (vs. SCE) during 4 hours at 298 K in order to study the changes occurred in the electrodes surfaces after a short ageing process. A 900 rpm electrode rotation rate was used for the EIS and chronoamperometric experiments, in order to prevent bubble formation that could obstruct the HER.

2.4. Ni electrode modification

The synthesis of both catalysts was carried out on a commercial nickel electrode with an area of 0.196 cm^2 (5 mm in diameter) mounted on a rotating disk electrode. The base nickel electrodes were mechanically polished with 0.05 μm alumina, degreased with ethanol and consecutively immersed in KOH (1 M), and HCl (10% w/w) solutions, during 1 minute, in order to decap the surface.

The synthesis of both catalysts was performed in an Autolab PGStat30 potentiostat / galvanostat coupled to a FRA2 module with a conventional two electrodes electrochemical cell thermostatically at 323 K (controlled with a Lauda Alpha RA 8 controller), using a massive nickel counter electrode with high area. During the process the working electrode was rotated at 1600 rpm to ensure the homogeneity of the electrodeposit [13].

The faradaic current applied during the synthesis of the catalysts, $NiTiO_{2dense}$ and $NiTiO_{2mesop}$, was −0.05 A cm^{-2} for 2700 s. After the synthesis, both catalysts were washed repeatedly with milli Q water in order to remove the rest of the electrodeposition bath.

4

3. Results and discussion

3.1. Structural characterization

Two types of TiO_2 particles were used as modifiers of the nickel structure. The first is commercial TiO_2 particulate (Fig. 1a). The second type of TiO_2 particles is a mesoporous TiO_2 synthesized by the aerosol method presented elsewhere (Fig. 1b) [21].

This material presents a mean size of ~500 nm in diameter. This average size was obtained from analyzing histograms constructed with at least 200 particles from the SEM micrographs with a 92% of sub-micrometric particles. The pore dimensions obtained from the isotherms are 3.5 nm for the diameter and 2.8 nm for the neck, with a surface area of 240 $m^2 g^{-1}$ [24].
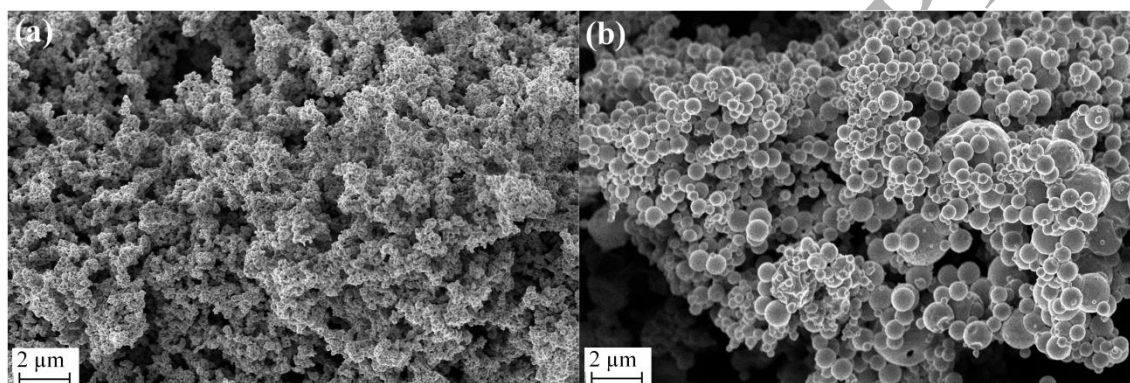

Fig. 1. SEM micrograph of the (a) commercial TiO_2 particles and (b) mesoporous TiO_2 particles used for the synthesis of the $NiTiO_{2dense}$ and $NiTiO_{2mesop}$, respectively.

SEM micrographs presented in Fig. 2 shows the surface structure of $NiTiO_{2dense}$ (Fig. 2a, b) and $NiTiO_{2mesop}$ (Fig. 2c, d) catalysts. It can be seen that both catalysts have a highly rough surface with aggregates of titanium particles distributed randomly. The aggregates present in the $NiTiO_{2mesop}$ catalyst are larger than those found in the $NiTiO_{2dense}$ catalyst, which is probably due to the mesoporous TiO_2 particles having larger size than those of dense TiO_2, which would generate larger agglomerates. In both catalysts it is observed, particularly at higher magnifications (Fig. 2b, d), that TiO_2 aggregates are not only present at the surface but they also exist in the bulk of the nickel matrix.
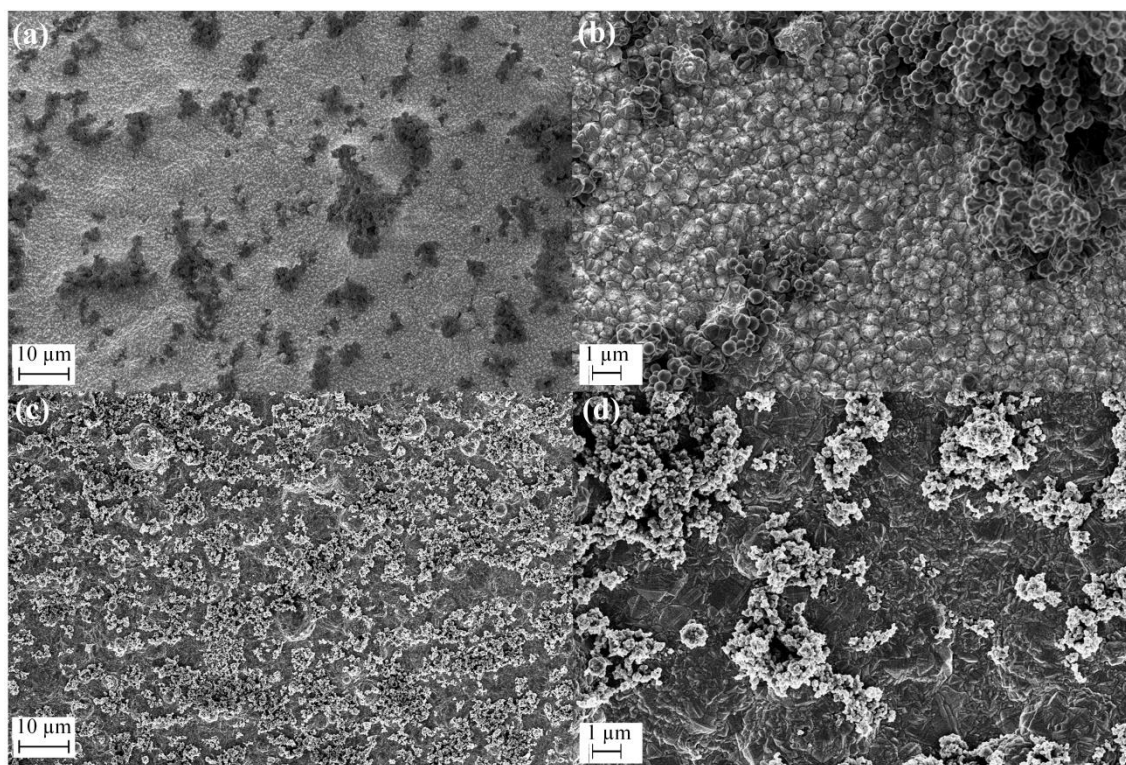
5

Fig. 2. SEM micrograph of the $NiTiO_{2mesop}$ (a and b) and $NiTiO_{2dense}$ (c and d).

EDX measurements confirm the presence of Ti and Ni in the catalyst matrix homogeneously distributed with around 2% Ti. The X-ray diffraction patterns of the $NiTiO_{2dense}$, $NiTiO_{2mesop}$ and a conventional nickel Watts catalyst [13] are indicated in Fig. 3(a). All the diffractograms show typical reflections of face cubic centered (fcc) structures of nickel. The diffraction parameters obtained are indicated in Table 1 for the Ni peaks observed in the diffractograms. Particularly, the $NiTiO_{2dense}$ shows signals corresponding to anatase TiO_2 [25] with low intensity (Fig. 3b). It has been widely reported in literature that the (1 1 1) plane is more stable than the (2 0 0) plane, probably because the (1 1 1) plane is more compact [26]. The (1 1 1)/(2 0 0) planes ratio is often used as one of the parameters related to the catalyst stability, with the stability being increased by increasing the value of the ratio. This (1 1 1)/(2 0 0) planes ratio for nickel Watts, $NiTiO_{2dense}$ and $NiTiO_{2mesop}$ has values of 4 without difference between the catalysts. The high value of the planes ratio indicates that the presence of titanium particles does not affect the stability of the nickel substrate.

Raman spectra of the different particles used for the catalyst synthesis along with the spectra of both catalysts ($NiTiO_{2dense}$ and $NiTiO_{2mesop}$) are presented in Fig. 3(c). It can be seen that commercial titanium particles have bands at 393, 512 and 636 cm^{-1} which can be all assigned to the anatase phase. No peaks related to rutile structure (138, 230, 443, 606 cm^{-1}) were observed in this sample [27], while the mesoporous TiO_2 particles do not present bands in Raman [28]. It is also observed in Fig. 3(c) the spectra of $NiTiO_{2dense}$ which is similar to those obtained for commercial TiO_2, with the absence of peaks corresponding to Ni oxides or nickel hydrides in any of the catalysts

6

[29]. Thus, the catalyst synthesis process did not generate appreciable changes in the structure of TiO_2 detectable by vibration of bands in the Raman spectra.
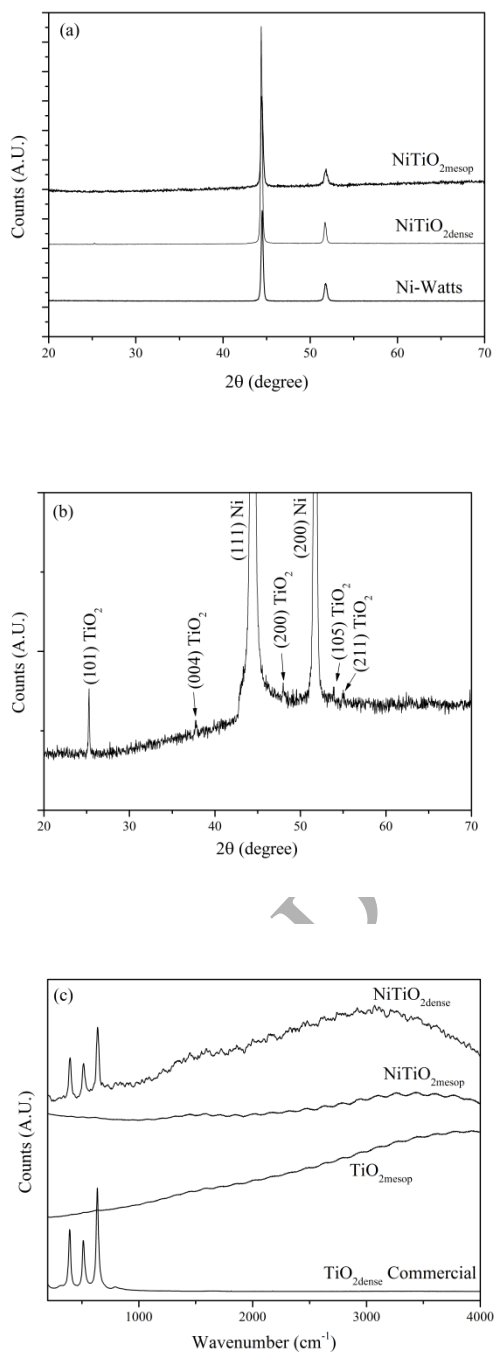

Fig. 3. (a) X-ray diffraction patterns of all the catalysts synthesized, (b) zoom of the XRD patter of the $NiTiO_{2dense}$ catalyst, (c) Raman spectra of the commercial TiO_2 particles, mesoporous TiO_2 particles, $NiTiO_{2dens}$e and $NiTiO_{2mesop}$.

3.2. Cyclic voltammetry and chronoamperometry

The cyclic voltammetries measured in $NiTiO_{2dense,}$ $NiTiO_{2mesop}$ and a conventional Ni-Watts catalyst are shown in Fig. 4. It can be seen that the three catalysts have similar onset potential of about −0.95 V (vs. SCE).However, there

7

is a noticeable increase in current density for HER at −1.5 V (vs. SCE) by incorporating TiO_2 into the catalyst structure. Particularly, the NiTiO$_{2mesop}$ catalyst has a current density 1.45 times greater than the measured with NiTiO$_{2dense}$ catalyst and 8.8 times greater than that presented by the conventional Ni-Watt catalyst. Differences in oxidation/reduction peaks of catalytic species (mainly nickel) can also be observed, with a marked increase in voltammograms related to the loading of the electric double layer of the electrodes. This increase of the peaks current is greater in the NiTiO$_{2mesop}$ catalyst that the NiTiO$_{2dense}$ catalyst and may be explained by the fact that the former has a greater accessible electrochemical area than that of NiTiO$_{2dense}$, resulting in a higher charge current of the double layer [30]. This increase in the current density at −1.5 V (vs. SCE) is directly related to the *j* increase observed in the chronoamperometric profiles of the ageing process presented in Fig. 5.
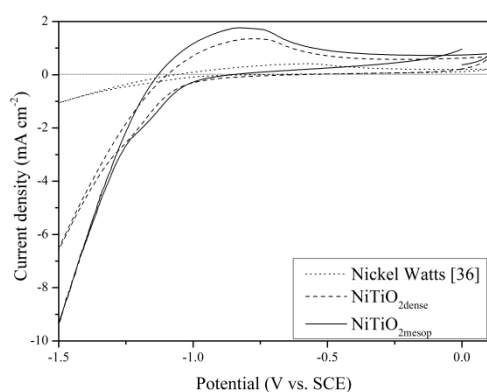

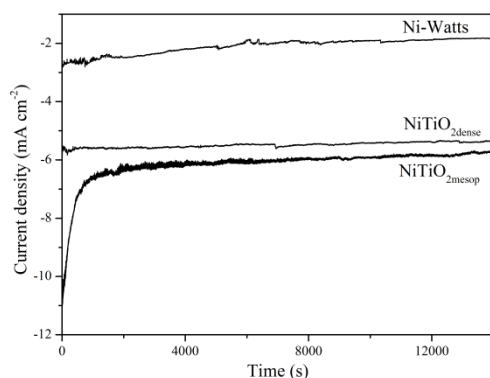**Fig. 4.** Cyclic voltammogram of bare nickel [35], NiTiO$_{2dense}$ and NiTiO$_{2mesop}$ measured at 10 mV s^{-1} and 298 K.

Fig. 5. Chronoamperometric profiles of bare nickel [35], NiTiO$_{2dense}$ and NiTiO$_{2mesop}$ measured at 298 K.

The electrode deactivation rate (δ) was calculated as [19,31]:

$$\delta = -\frac{100}{j_e}\left(\frac{dj}{dt}\right) \tag{3}$$

8

where j_e is the current extrapolated at the start of polarization, and the slope, dj/dt, is evaluated from the linear decay at $t > 2000$ s. The deactivation rate of each electrode is presented in Table 2. It can be seen that the rate of deactivation of the electrode decreases considerably with the addition of TiO_2 to the catalyst matrix. Differences are observed between this effect from $NiTiO_{2dense}$ and $NiTiO_{2mesop}$, where nickel containing mesoporous particles has a higher decay rate than $NiTiO_{2dense}$. This differences may be due to both catalysts ($NiTiO_{2dense}$ and $NiTiO_{2mesop}$) having more stable structures than those of Ni-Watts, although $NiTiO_{2mesop}$ has a larger exposed area which would increase the surface deactivation rate. In addition to this, after the ageing process, Raman bands at 3581 and 3660 cm^{-1} corresponding to the presence of surface nickel hydrides are not observed for the $NiTiO_2$ hybrid catalysts. These hydrides are normally detected by Raman on pure nickel catalysts after this type of ageing treatment [13].

Fig. 5 shows that the $NiTiO_{2mesop}$ catalyst during the first few minutes of hydrogen generation has much higher currents than the other catalysts studied and takes about 2000 seconds to stabilize, unlike the $NiTiO_{2dense}$ and Ni-Watts that do so during the first few seconds of the chronoamperometric experiment. This effect has already been observed previously during the electrochemical use of other mesoporous materials [30,32] and could be due to the lower diffusion coefficient of the species within the mesopores [33,34]. However, in spite of this lower diffusion coefficient, the $NiTiO_{2mesop}$ catalyst shows higher current density than those presented by the other catalysts.

Fig. 6(a) shows the cyclic voltamograms of $NiTiO_{2dense}$ and $NiTiO_{2mesop}$ catalysts measured at 298 K before and after the short ageing process. After ageing, the $NiTiO_{2dense}$ catalyst shows a 16 % decrease in current density while in the $NiTiO_{2mesop}$ catalyst shows an increase of 31% in current density. This indicates that the $NiTiO_{2mesop}$ catalyst has not only greater catalytic activity than that of $NiTiO_{2dense}$ but also undergoes an activation process after ageing, an effect sometimes shown by other catalysts in the literature [23,38].

Tafel curves constructed for these catalysts before and after ageing are shown in Fig. 6(b). It is observed that after ageing the $NiTiO_{2dense}$ catalyst increases its equilibrium potential while the $NiTiO_{2mesop}$ catalyst maintains it. Calculated Tafel slope values are between 0.13 and 0.15 V dec^{-1} for $NiTiO_{2mesop}$ and $NiTiO_{2dense}$, respectively (Table 2). The values are similar to that reported for commercial bare Ni (0.13 V dec^{-1}) [35,36], and are consistent with a Volmer reaction as the rate determining step in the global reaction where the Tafel slopes corresponds to the electron transfer (with a theoretical Tafel slope of ~0.12 V dec^{-1}).

It is noticed that the Ni-Watts and $NiTiO_{2dense}$ catalysts freshly synthesized have similar values, while the $NiTiO_{2mesop}$ catalyst shows a 45% higher exchange current. After ageing, Ni-Watts and $NiTiO_{2dense}$ catalysts reduce their exchange current. Particularly a strong decrease of the j_0 in the Ni-Watts catalyst is observed, much higher than that observed in $NiTiO_{2dense}$. Additionally, after ageing, the $NiTiO_{2mesop}$ catalyst shows an increase in the exchange

current of one magnitude order. These modifications in the exchange current are reflected in the changes observed in the potentiodynamic experiments (Figs 4 and 6a).
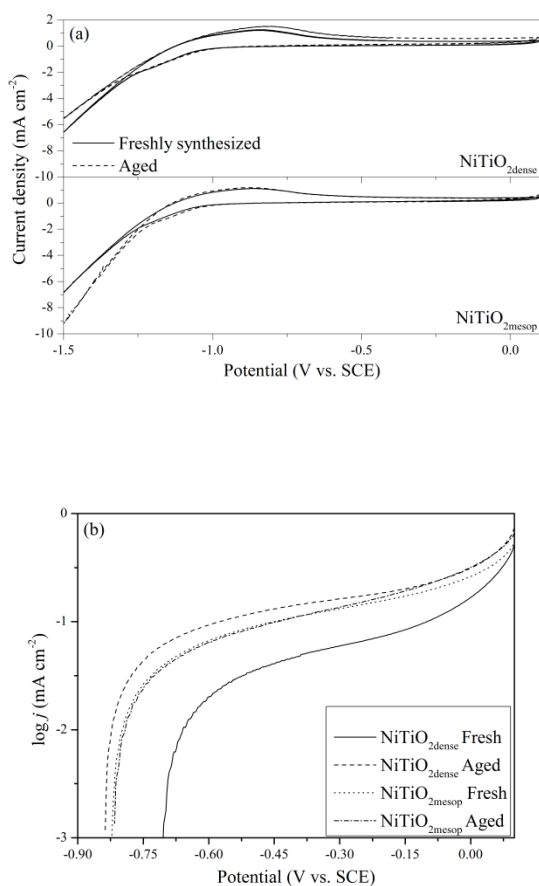

Fig. 6. (a) Cyclic voltammogram of $NiTiO_{2dense}$ and $NiTiO_{2mesop}$ measured at 10 mV s^{-1} and 25 °C, before and after the short ageing process. (b) Tafel plots for the HER on fresh and aged catalysts measured at 293 K. Scan rate = 10 mV s^{-1}.

3.3. Electrochemical impedance spectroscopy analysis

It has been reported numerous times in the literature that the HER on nickel electrodes in alkaline medium can be adjusted using the Armstrong & Henderson equivalent circuit (AHEC) [37,38]. This model describes that the HER can be adjusted by two circles in the complex plane dependent on the applied overpotential [39,40]. However the AHEC model does not fit particularly well when the electrode is porous or possess high roughness [41], and it is necessary to modify it by the addition of constant phase elements (CPE), since experimentally only a single flattened semicircle is observed. It has been presented in literature that the use of the CPE on rough electrodes is necessary due to capacitance dispersion [42]. The AHEC model modified with a CPE (denoted as AHEC1CPE) describes a simple hydrogen evolution process, found usually on polycrystalline Ni and some porous Ni based electrodes [43–45].

10

The AHEC modified by two-CPE (denoted as AHEC2CPE) theoretically produces on the complex-plane plot two semicircles, with the high frequency semicircle related to the porosity, and the low-frequency semicircle related to the charge-transfer process [46–49]. Moreover, on porous electrodes the high frequency part of the complex plane plots usually shows either straight line at 45° or a semicircle for cylindrical or pear shape pores, respectively [50]. In a similar way, in several works it has been proposed the use of a modified Randles model using a CPE (denoted as Randles-CPE) to correctly adjust the experimental data [39,47].

In this work we have applied several models to adjust the experimental data, such as those presented in Fig. 7. Thus, we used the conventional AHEC, a modified AHEC with a CPE (AHEC1CPE), a modified AHEC with 2 CPE (AHEC2CPE), a model containing 2 CPE in series (2CPE) [39], a conventional Randles model and a model Randles modified with a CPE (Randles-CPE).

It was taken as a setting parameter the χ^2 with values lower than 0.01 as the best models for fitting. Fig. 7 shows an example of a Nyquist graph adjusted by the different models along with the χ^2 value obtained for the adjustment.

In this way the C_{dl}, R_{ct} and R_p parameters were obtained for the different models.

A very good approximation to the experimental data for the all electrodes was obtained using the AHEC2CPE, the 2CPE electrical circuit and the Randles-CPE model. However, for potentials where the hydrogen generation reaction occurs, the AHEC1CPE model also fits properly. On the other hand, it is important to clarify that the Randles-CPE model only adjusts the first semicircle, unlike the other models derived from the Armstrong & Henderson model.

Fig. 8 shows the impedance spectra in the complex plane for the NiTiO$_{2dense}$ and NiTiO$_{2mesop}$ catalysts measured at 25°C and different potentials. It can be seen that increasing the overpotential systematically decreases the radius of the Nyquist plot indicating a dependence of the charge transfer resistance with the overpotential.

In Table 3 the values obtained for the models having the best fits are shown, (AHEC2CPE and Randles-CPE). Particularly, the AHEC2CPE model presents a better R_{ct} adjustment where it can be seen that it decreases significantly in the NiTiO$_{2mesop}$ catalyst with respect to NiTiO$_{2dense}$, indicating that the increase in the catalytic activity is not only due to an increase in the surface area of the electrode, but also there is an increased catalytic effect on the catalyst synthesized using mesoporous TiO$_2$.

The Randles-CPE model can only be used to fit the first half-circle of the Nyquist plot which is commonly associated to the roughness of the surface [46]. It can be seen that there are differences between the values obtained for the different catalysts although they seem to indicate that the NiTiO$_{2dense}$ catalyst has a higher roughness factor than NiTiO$_{2mesop}$, strengthening the hypothesis that the NiTiO$_{2mesop}$ catalyst is more electroactive regardless of differences in surface area.
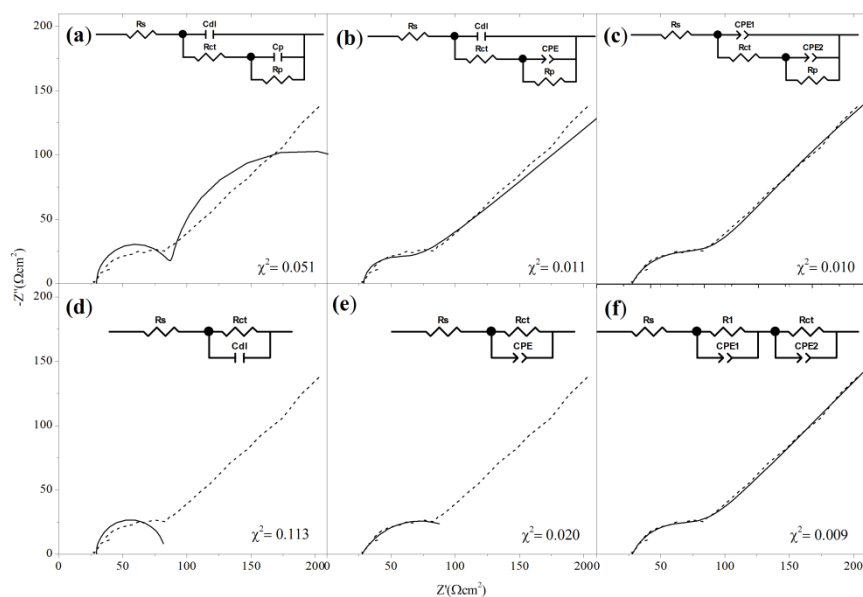
Fig. 7. NiTiO$_{2mesop}$ measured at 25 °C and −1.105 V (vs. SCE) adjusted with the equivalent circuit models: (a) AHEC, (b) AHEC1CPE, (c) AHEC2CPE, (d) Randles model, (e) Randles-CPE model and (f) 2CPE model.
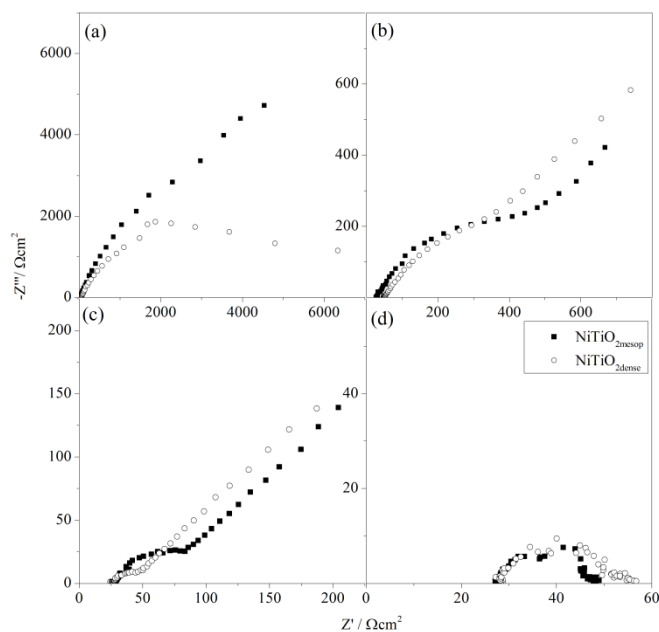

Fig. 8. Nyquist plot impedance spectra in the complex plane for the HER on NiTiO$_{2mesop}$ in 1 M KOH at 298 K and at a rotation rate of 900 rpm measured at: (a) −0.5 V (vs. SCE), (b) −0.95 V (vs. SCE), (c) −1.05 V (vs. SCE) and (d) −1.25 V (vs. SCE).

In the analysis of the Nyquist graphs at high frequencies (not showed) it is observed that all impedance spectra for both catalysts, regardless of the applied overpotential, has a straight line at 45° with respect to the real axis. This behavior has been attributed numerous times in the literature to the presence of surface roughness, particularly to the presence of surface pores [14,44,46]. It is common to see on porous electrodes that the high frequency part of the complex plane plots shows a straight line at 45°. Keiser et al. [51] studied the impedance of shaped pores in the absence of a faradaic process and found that a straight line at 45° is observed for cylindrical pores at high frequencies. These features are due to geometric effects, and are related to the coupling of the double-layer capacitance and the solution resistance in pores, detected at high frequencies.

4. Conclusions

In this work a simple and reproducible method for the synthesis of modified nickel catalysts with TiO_2 particles by electrodeposition has been presented. These modified catalysts show to have a higher catalytic activity than the Nickel-Watts catalyst and in particular the catalyst synthesized using mesoporous TiO_2 has a higher catalytic activity than that synthesized using dense TiO_2. Additionally, it was found that the nickel catalyst modified with mesoporous TiO_2 presents an increase in the catalytic activity after the ageing process in alkaline medium. The Tafel slope values indicate that the rate-determining step of the reaction is the Tafel reaction with one electron. The adjustment of the measured data by electrochemical impedance spectroscopy using different equivalent circuits was analyzed. As expected, the models using circuits with a larger number of fitting parameters present the best adjustments, although a satisfactory fitting can be obtained with the modified Randles model with CPE and the model proposed by Armstrong & Henderson modified with 1 CPE. The need to use a CPE to obtain an appropriate fit has been presented numerous times in the literature as an indication of the roughness of the electrode. Spectroscopic Raman analysis indicates that the presence of TiO_2 in the catalyst matrix inhibits the formation of surface nickel hydrides at least in short ageing times. In this work we have found that the $NiTiO_2$ hybrid catalyst employing mesoporous TiO_2 particles can be synthesized by a simple method and exhibit superior catalytic activity and stability than the Ni-Watt catalysts commonly used in both conventional and zero gap electrolyzers using alkaline electrolyte.

References

[1] T.K. Mandal, D.H. Gregory, Proc. Inst. Mech. Eng. Part. C. J. Mech. Eng. Sci. 224 (2010) 539–558.

[2] I.P. Jain, Int. J. Hydrogen Energ. 34 (2009) 7368–7378.

[3] N.A. Kelly, T.L. Gibson, M. Cai, J.A. Spearot, D.B. Ouwerkerk, Int. J. Hydrogen Energ. 35 (2010) 892–899.

[4] S. Elnashaie, Z.X. Chen, P. Prasad, Int. J. Green Energy 4 (2007) 249–282.

[5] W. Sheng, H.A. Gasteiger, Y. Shao-Horn, J. Electrochem. Soc. 157 (2010) B1529-B1536.

[6] X. Zou, Y. Zhang, Chem. Soc. Rev. 44 (2015) 5148–5180.

[7] A. Lasia, A. Rami, J. Electroanal. Chem. 294 (1990) 123–141.

[8] J.R. McKone, B.F. Sadtler, C.A. Werlang, N.S. Lewis, H.B. Gray, ACS Catal. 3 (2013) 166–169.

[9] L. Chen, A. Lasia, J. Electrochem. Soc. 138 (1991) 3321–3328.

[10] C. Fan, D.L. Piron, A. Sleb, P. Paradis, J. Electrochem. Soc. 141 (1994) 382–387.

[11] Q. Liu, J. Tian, W. Cui, P. Jiang, N. Cheng, A.M. Asiri, X. Sun, Angew. Chem. Int. Ed. 53 (2014) 6710–6714.

[12] Y. Liang, Y. Li, H. Wang, H. Dai, J. Am. Chem. Soc. 135 (2013) 2013–2036.

[13] E.A. Franceschini, G.I. Lacconi, Electrocatalysis 9 (2017) 47–58.

[14] B. Losiewicz, A. Budniok, E. Rowinski, E. Lagiewka, A. Lasia, Int. J. Hydrogen Energ. 29 (2004) 145–157.

14

[15] C. Ravichandran, D. Vasudevan, P.N. Anantharamn, J. Appl. Electrochem. 22 (1992) 179–181.

[16] X. Chen, S. Shen, L. Guo, S.S. Mao, Chem. Rev. 110 (2010) 6503–6570.

[17] J. Yang, D. Wang, H. Han, C. Li, Acc. Chem. Res. 46 (2013) 1900–1909.

[18] L. Elias, A.C. Hegde, RSC Adv. 6 (2016) 66204-66214.

[19] E.A. Franceschini, M.M. Bruno, F.J. Williams, F.A. Viva, H.R. Corti, ACS Appl. Mater. Inter. 5 (2013) 10437–10444.

[20] L. Mahoney, S. Rasalingam, R.T. Koodali, in: D. Kilin (Ed.), Photoinduced Processes at Surfaces and in Nanomaterials, ACS Symposium Series, Washington DC., 2015, pp 81–101.

[21] G.J.A.A. Soler-Illia, A. Zelcer, M.V. Lombardo, E.A. Franceschini, Un procedimiento para la obtención de partículas esféricas de oxidos metalicos mesoporosos de composición, area superficial, porosidad y tamaño controlados. Patent: 20150104299, 2015.

[22] J. Rodríguez-Carvajal, Physica B 195 (1993) 55–69.

[23] E.A. Franceschini, G.I. Lacconi, H.R. Corti, Int. J. Hydrogen Energ. 41 (2016) 3326–3338.

[24] M.I. Velasco, M.B. Franzoni, E.A. Franceschini, E. González Solveyra, D. Scherlis, R.H. Acosta, G.J.A.A. Soler-Illia, J. Phys. Chem. C. 121 (2017) 7533–7541.

[25] X. Wei, G. Zhu, J. Fang, J. Chen, Int. J. Photoenergy 2013 (2013) 1–6.

[26] P. Quaino, F. Juarez, E. Santos, W. Schmickler, Beilstein J. Nanotechnol. 5 (2014) 846–854.

[27] D. Fang, K. Huang, S. Liu, J. Huang, J. Braz. Chem. Soc. 19 (2008) 1059–1064.

[28] M.J. Henderson, A. Gibaud, J.F. Bardeaub, J.W. White, J. Mater. Chem. 16 (2006) 2478–2484.

[29] D.S. Hall, D.J. Lockwood, S. Poirier, C. Bock, B.R. MacDougall, ACS Appl. Mater. Inter. 6 (2014) 3141–3149.

[30] M.M. Bruno, E.A. Franceschini, F.A. Viva, Y.R.J Thomas, H.R. Corti, Int. J. Hydrogen Energ. 37 (2012) 14911–14919.

[31] M.M. Bruno, E.A. Franceschini, G.A. Planes, H.R. Corti, J. Appl. Electrochem. 40 (2010) 257–263.

[32] R.S. Amin, A.E. Fetohi, R.M. Abdel Hameed, K.M. El-Khatib, Int. J. Hydrogen Energ. 41 (2016) 1846–1858.

[33] R. Takahashi, S. Sato, T. Sodesawa, H. Nishida, Phys. Chem. Chem. Phys. 4 (2002) 3800−3805.

[34] R. Takahashi, S. Sato, T. Sodesawa, H. Nishida, J. Ceram. Soc. Jpn. 109 (2001) 840−845.

[35] E.A. Franceschini, G.I. Lacconi, H.R. Corti, Electrochim. Acta 2015, 159, 210–218.

[36] G. Kreysa, B. Hakansson, P. Ekdunge, Electrochim. Acta 33 (1988) 1351−1357.

[37] R.D. Armstrong, M. Henderson, J. Electroanal. Chem. 39 (1972) 81–90.

[38] E.A. Franceschini, G.I. Lacconi, H.R. Corti, J. Energy Chem. 26 (2017) 466–475

[39] E. Daftsis, N. Pagalos, A. Jannakoudakis, P. Jannakoudakis, E. Theodoridou, R. Rashkov, M. Loukaytsheva, N. Atanassov, J. Electrochem. Soc. 150 (2003) C787-C793.

[40] J. Panek, A. Serek, A. Budniok, E. Rowinski, E. Lagiewka, Int. J. Hydrogen Energ. 28 (2003) 169–175.

[41] C. Hitz, A. Lasia, J. Electroanal. Chem. 500 (2001) 213–222.

[42] Z. Kerner, J. Pajkossy, Electrochim. Acta 46 (2000) 207–211.

[43] A. Lasia, A. Rami, J. Electroanal. Chem. 294 (1990) 123–141.

[44] A. Lasia, Curr. Top. Electrochem. 2 (1993) 239–251.

[45] L. Chen, A. Lasia, J. Electrochem. Soc. 138 (1991) 3321–3328.

[46] A. Lasia, in: B.E. Conway, R.E. White (Eds.), Modern Aspects of Electrochemistry, Kluwer Academic/Plenum Publishers, New York, 2002, pp. 1–49.

[47] J. Panek, A. Serek, A. Budniok, E. Rowinski, E. Lagiewka, Int. J. Hydrogen Energ. 28 (2003) 169–175.

[48] R. Karimi Shervedani, A. Lasia, J. Electrochem. Soc. 144 (1997) 2652–2657.

[49] R. Karimi Shervedani, A. Lasia, J. Appl. Electrochem. 29 (1999) 979–986.

[50]A. Lasia, in: B.E. Conway, R.E. White (Eds.), Modern Aspects of Electrochemistry, Kluwer Academic/Plenum Publishers, New York, 1999. 143-248.

[51] H. Keiser, K.D. Beccu, M.A. Gutjahr, Electrochim. Acta, 21 (1976) 539–543.

Tables

Table 1. XRD parameters: Peak position (2θ), full width at half maximum (FWHM), crystal size and *d* spacing for the peaks observed on the synthesized catalysts

	2 Theta (degree)	FWHM (degree)	Crystal size (nm)	*d* (Å)	Plane
Ni-Watts	44.47	0.26	34.2	2.03	(111)
Ni-Watts	51.76	0.37	25.2	1.76	(200)
$NiTiO_{2mesop}$	44.43	0.29	31.0	2.03	(111)
$NiTiO_{2mesop}$	51.78	0.45	20.5	1.76	(200)
$NiTiO_{2dense}$	44.38	0.21	42.5	2.04	(111)
$NiTiO_{2dense}$	51.69	0.29	31.8	1.76	(200)

Table 2. Deactivation rate (δ), Tafel slope (*b*), and exchange current density (j_0).

	δ (s^{-1})	b^a (mV dec^{-1})	b^b (mV dec^{-1})	$j_0{}^a$ (mA cm^{-2})	$j_0{}^b$ (mA cm^{-2})
Ni Watts [13]	4.9×10^{-3}	0.256	0.142	1.20×10^{-4}	6.91×10^{-7}
$NiTiO_{2dense}$	3.6×10^{-4}	0.149	0.146	1.20×10^{-4}	6.15×10^{-5}
$NiTiO_{2mesop}$	6.6×10^{-4}	0.135	0.130	1.75×10^{-4}	2.52×10^{-3}

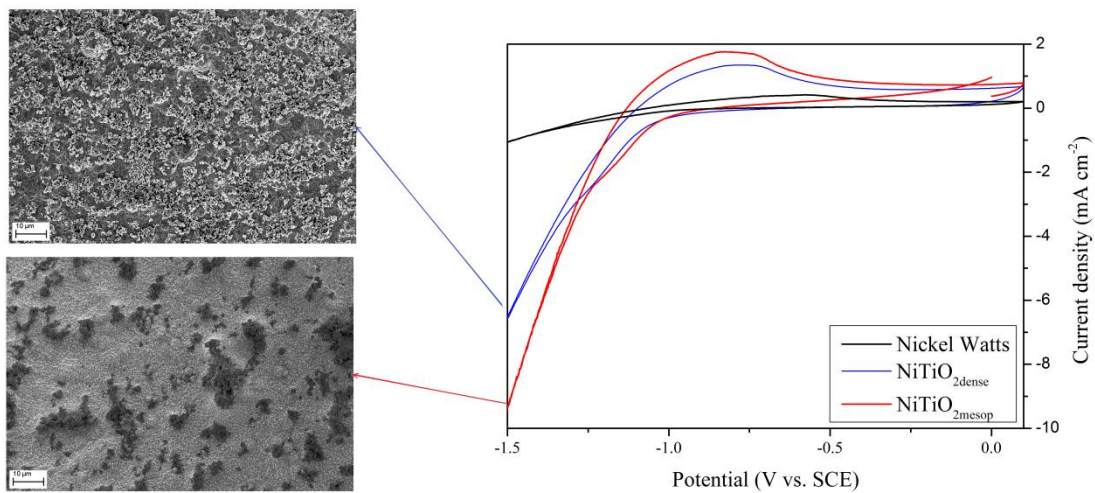[a] Fresh synthesized catalyst, [b] aged catalyst.

Table 3. Parameters of the AHEC2CPE and the Randles-CPE for the HER in 1 M KOH at 298 K for all the synthesized catalysts at −1.05 V (vs. SCE).

AHEC2CPE	$NiTiO_{2dense}{}^a$	$NiTiO_{2dense}{}^b$	$NiTiO_{2mesop}{}^a$	$NiTiO_{2mesop}{}^b$
R_s	48.4	20.19	27.473	37.41
CPE1	0.001774	0.02898	0.01355	0.022025
R_{ct}	1803	1465	541.6	588.2
CPE2	0.020491	0.002778	0.001276	0.002137
R_p	16.42	30.05	41.63	69.36
Randles-CPE				
R_s	48.13	19.84	27.32	36.98
CPE	0.0032027	0.0040133	0.00176	0.00277
R_{ct}	36.35	52.31	91.03	106.9

[a] Fresh synthesized catalyst, [b] aged catalyst.

Graphical Abstract

Hybrid Ni/TiO$_2$ catalysts were synthesized by a simple and reproducible method. These modified catalysts show to have a higher catalytic activity than Nickel-Watts catalyst. The catalyst synthesized using mesoporous TiO$_2$ has the higher catalytic activity.

20